APOLD1 loss causes endothelial dysfunction involving cell junctions, cytoskeletal architecture, and Weibel-Palade bodies, while disrupting hemostasis

Simon Stritt,[1*] Paquita Nurden,[2*] Alan T. Nurden,[2] Jean-François Schved,[3] Jean-Claude Bordet,[4] Maguelonne Roux,[5] Marie-Christine Alessi,[6] David-Alexandre Trégouët,[5,7] Taija Mäkinen[1] and Muriel Giansily-Blaizot[3]

[1]Department of Immunology, Genetics and Pathology, Uppsala University, Uppsala, Sweden; [2]Institut de Rythmologie et de Modélisation Cardiaque, Hôpital Xavier Arnozan, Pessac, France; [3]Department of Biological Hematology, CHU Montpellier, Université de Montpellier, Montpellier, France; [4]Hematology, Hospices Civils de Lyon, Bron Biology Center and Hemostasis-Thrombosis, Lyon-1 University, Lyon, France; [5]Laboratory of Excellence GENMED (Medical Genomics), Paris, France; [6]Aix Marseille University, INSERM, INRAE, C2VN, Marseille, France and [7]University of Bordeaux, INSERM, Bordeaux Population Health Research Center, U1219, Bordeaux, France.

Correspondence:
S. Stritt
simon.stritt@igp.uu.se

P. Nurden
paquita.nurden@gmail.com.

Received: February 7 2022.
Accepted: May 10, 2022.
Early view: May 31, 2022.

https://doi.org/10.3324/haematol.2022.280816

SUPPLEMENTAL METHODS

Cell culture

Primary human dermal microvascular endothelial cells (HDMECs) from juvenile foreskin were obtained from PromoCell (C12210). Cells were maintained in cell culture dishes coated with 0.2 µg cm^{-2} bovine fibronectin (F1141, Sigma-Aldrich) supplied with complete Endothelial Cell Growth Medium 2 (ECGMV2; C-22022, PromoCell). At 90% confluency HDMECs were gently detached with Accutase (A6964, Sigma-Aldrich), washed with complete medium and incubated for 45 min at 4°C with rat anti-human podoplanin antibody-coated (NZ-1, 14-9381-82, Thermo-Fisher Scientific, 7 µg per 100 mm dish) Dynabeads (11035, Thermo-Fisher Scientific) and subsequently separated into bead-bound lymphatic and unbound blood ECs by magnetic sorting. Purity was assessed by immunolabeling for PDPN and PROX1. Cells were maintained at 37 °C and 5% CO_2. Purified human dermal blood ECs (HDBECs) were maintained in cell culture dishes coated with 0.2 µg cm^{-2} bovine fibronectin (F1141, Sigma-Aldrich) in complete Endothelial Cell Growth Medium 2 (ECGMV2; C-22022, PromoCell) and passaged at 90% confluency using Trypsin-EDTA (25300-054, Thermo-Fisher Scientific). For the indicated experiments fusion of lysosomes and autophagosomes was inhibited by treatment with 25 µM chloroquine (dissolved in ddH_2O; C6628, Sigma-Aldrich).

Platelet preparation

Blood samples of patients were obtained after informed consent in accordance with the declaration of Helsinki. Ethical approval was obtained in France from INSERM (RBM 04–14) for the national project 'Network on the inherited diseases of platelet function and platelet production'. Fresh blood samples of patients and healthy volunteers were collected in 1/10 volume of acid-citrate-dextrose and centrifuged for 10 min at 200 g. Platelet-rich plasma (PRP) was collected, supplemented with 3 µL of apyrase (0.02 U mL^{-1}, A6410, Sigma-Aldrich) and 5 µL Prostacyclin I_2 (PGI_2) (0.1 µg mL^{-1}, P6188, Sigma-Aldrich) per mL PRP. Before adherence to poly-L-lysine (PLL, P8920, Sigma-Aldrich)-coated slides, platelets were pelleted by centrifugation for 10 min at 800 g and washed twice with Tyrode-N-2-hydroxyethyl-piperazine-N′2-ethanesulfonic acid (HEPES) buffer (134 mM NaCl, 0.34 mM Na_2HPO_4, 2.9 mM KCl, 12 mM $NaHCO_3$, 5 mM HEPES, 5 mM glucose, 0.35% bovine serum albumin (BSA), pH 7.4) containing 2 µL mL^{-1} apyrase and 5 µL mL^{-1} PGI_2. Subsequently samples were resuspended at 2 x

10^5 platelets μL^{-1} in Tyrode-HEPES buffer containing 2 µL mL^{-1} apyrase and 5 µL mL^{-1} PGI_2 and were allowed to rest for 30 min at 37 °C prior to being used in experiments.

Immunolabeling of resting platelets and HDBECs

For platelet studies coverslips were coated with PLL overnight at 4 °C. Platelets were allowed to adhere for 20 minutes, fixed in PHEM buffer (60 mM piperazine-N,N-bis-2- ethanesulfonic acid (PIPES), 25 mM HEPES, 10 mM EGTA, 2 mM $MgCl_2$, pH 6.9) supplemented with 4% PFA, permeabilized and blocked with 0.1% IGEPAL CA-630 (I8896, Sigma-Aldrich), 3% bovine serum albumin (BSA, A3295, Sigma-Aldrich) in PBS and stained with the indicated primary antibodies. HDBECs were processed in a similar manner, but were grown on 0.2 µg cm^{-2} bovine fibronectin-coated (F1141, Sigma-Aldrich) coverslips. The following primary antibodies were used for immunofluorescence staining: rat anti-CD41 (3.33 µg mL^{-1}, 14-0411-82 (MWReg30), Thermo-Fisher Scientific), rabbit anti-APOLD1 C-term (5.0 µg mL^{-1}, ab105079, Abcam), rabbit anti-VWF (3.33 µg mL^{-1}, A0082, DAKO), goat anti-VE-Cad (0.67 µg mL^{-1}, sc-6458 (C-19), Santa-Cruz Biotechnology), rabbit anti-claudin 5 (3.33 µg mL^{-1}, 34-1600, Thermo-Fisher Scientific), mouse anti-FN (5.0 µg mL^{-1}, F6140, Sigma-Aldrich), mouse anti-VE-Cad (0.67 µg mL^{-1}, sc-9989 (F-8), Santa-Cruz Biotechnology), mouse anti-CD31 (2.5 µg mL^{-1}, M0823, DAKO), goat anti-ANGPT2 (2.5 µg mL^{-1}, AF623, R&D Systems), mouse anti-VWF (0.67 µg mL^{-1}, sc-53466 (F-8/86), Santa-Cruz Biotechnology), mouse anti-CD62P (5.0 µg mL^{-1}, sc-8419 (CTB201), Santa-Cruz Biotechnology), mouse anti-CD63 (3.33 µg mL^{-1}, 10628D (Ts63), Thermo-Fisher Scientific), mouse anti-LAMP1 (5.0 µg mL^{-1}, #15665 (D4O1S), Cell Signaling Technology), mouse anti-RAB7 (5.0 µg mL^{-1}, #95746 (E9O7E), Cell Signaling Technology), mouse anti-LC3B (5.0 µg mL^{-1}, #83506 (E5Q2K), Cell Signaling Technology), and mouse anti-SQSTM1 (5.0 µg mL^{-1}, ab56416, Abcam. Filamentous actin was labeled with phalloidin-Atto647N (170 nM, AD 647N-82, Atto-Tec). After extensive washes with PBS primary antibodies were detected with suitable fluorophore-conjugated secondary antibodies (Jackson Immuno-Research) at a concentration of 3.75 µg mL^{-1}. All samples were either mounted with Fluoroshield with (F-6057, Sigma-Aldrich) or without (F6182, Sigma-Aldrich) DAPI (4′,6-diamidino-2-phenylindole) and visualized by confocal microscopy.

Transmission electron microscopy (TEM)

TEM was performed with support of the BioVis EM facility (Uppsala University, Sweden). Briefly, confluent control and *APOLD1*-silenced HDBECs were grown in a 6-well plate, fixed with 2.5% glutaraldehyde and 1% PFA in PIPES buffer pH 7.4, post-fixed in OsO_4 (O001, TAAB), dehydrated in ethanol and embedded in Agar 100 resin (AGR1045, Agar Scientific). 60 nm thick sections were prepared with a Leica EM UC7 ultramicrotome (Leica Microsystems) and stained with 2 % uranyl acetate and lead citrate. Samples were visualized using a Tecnai 12 BioTwin TEM (FEI Europe) equipped with a Gatan Orius CCD camera (Blue Scientific) at 80 kV.

Immunogold electron microscopy

ECs were grown on polycarbonate cell culture inserts (0.4 µm pore size, 140660, Thermo Fisher Scientific), fixed with 8% paraformaldehyde supplemented with 0.2% glutaraldehyde (Electron Microscopy Sciences, EMS, Hatfield, PA) and 0.2% sodium metaperiodate added extemporaneously in a 0.2 M sodium cacodylate buffer pH 7.4. Cells were washed with 0.2 M cacodylate - 0.4 M saccharose solution, dehydrated in graded ethanol and embedded in pure LR-White. Sections (70 nm thick) were cut using a Reichert Ultracut microtome (Leica Microsystems, Wetzlar, Germany), mounted on 200 mesh nickel grids (EMS) coated with 1:1000 polylysine. Non-specific sites were blocked (1% BSA + 1% normal goat serum in 50 mM Tris-HCl pH 7.4, 20 min at RT). Antibody incubations were carried out overnight at RT in buffer with rabbit IgG anti-VWF (3.3 µg mL^{-1}) and anti-APOLD1 (5 µg mL^{-1}) antibodies or a non-immune rabbit IgG dilution (negative control). *APOLD1*-silenced HDBEC monolayers were used as negative control for the immunogold labeling. Sections were washed three times (50 mM Tris-HCl) and incubated at RT (45 min) with 10 nm diameter gold particle-conjugated goat anti-rabbit Ig (Aurion, Wageningen, The Netherlands). Samples were washed three times (50 mM Tris-HCl pH 7.4 and distilled water) and fixed with 4% glutaraldehyde (3 min). Sections were stained with 5% uranyl acetate and observed with a transmission electron microscope 1400 JEM (JEOL, Tokyo, Japan), equipped with an Orius 600 Gatan camera and the Digital Micrograph software (Gatan, Pleasanton, CA) (Lyon Bio Image, Centre d'Imagerie Quantitative de Lyon Est, France).

Gene silencing

Short interference RNA (siRNA) treatments were performed according to the manufacturer's protocol using 4 different siRNAs targeting *APOLD1* (FlexiTube GeneSolution #GS81575, Qiagen). The used target sequences of *APOLD1* were: APOLD1 #2: 5'-AACGGTGCCTCTGTTACTTAA-3'; APOLD1 #3: 5'-GCCCGTGAAGCCGTCATCTAA-3'; APOLD1 #4: 5'-AAGACGGGAGAGAGGTATTTA-3'; APOLD1 #5: 5'-CACCCTGTTGTGAGATATTAA-3'. Target sequences of *ATG5* and *ATG7* were: ATG5 #6 5'-AACCTTTGGCCTAAGAAGAAA-3'; ATG7 #5 5'-ATCAGTGGATCTAAATCTCAA-3'. For efficient silencing, cells were subjected to two consecutive rounds of transfection at 0 h and 24 h using Lipofectamine 2000 (11668019, Thermo-Fisher Scientific). AllStars Negative Control siRNA (1027281, Qiagen) was used as control. After initial validation of all four APOLD1 siRNAs, that gave a similar phenotype irrespective of the siRNA used, subsequent studies were performed using APOLD1 #5 (SI00365141, Qiagen) siRNA. For ATG5 and ATG7 pre-validated siRNAs were purchased. Cells were analyzed 96 h after the first round of transfection if not stated otherwise.

Gene expression analysis

For qRT-PCR analysis of HDBECs, total RNA was isolated using the RNeasy Mini or Micro kit (74104/74004, Qiagen) and 1 µg was reverse transcribed with the help of SuperScript VILO (11755050, Thermo-Fisher Scientific). Of note, genomic DNA was digested by RNase free DNaseI (79254, Qiagen) treatment for 15 min at RT. Subsequently, relative gene expression was quantified using FAM-MGB-conjugated TaqMan Gene Expression Assays (Applied Biosystems) and a StepOnePlus Real-Time PCR System (4376600, Thermo-Fisher Scientifc). *APOLD1*, *ATG5*, *ATG7*, expression levels were normalized to *GAPDH*. The following probes were used: Hs99999905_m1 *GAPDH*, Hs00169468_m1 *ATG5*, Hs04969948_m1 *ATG7*, and Hs00707371_s1 *APOLD1*.

In vitro permeability assay

36 h after the first round of transfection cells were detached using Accutase and each 4 x 10^4 control and *APOLD1*-silenced HDBECs were seeded in complete ECGMV2 on 0.2 µg cm^{-2} bovine fibronectin-coated Transwell inserts with a pore size of 0.4 µm (Costar 3413, Corning). 96 h after the first round of transfection 0.25 mg mL^{-1} 40 kDa FITC-dextran (FD40, Sigma-Aldrich) was added to the upper reservoir of the transwell inserts. After 30 min inserts were carefully removed, fixed by the addition of

4% PFA in PHEM buffer and processed for VE-Cad and phalloidin immunolabeling to control for monolayer integrity. Transcellular diffusion was determined by measuring FITC-dextran fluorescence in the lower chamber with a microplate reader (Synergy™ HTX Multi-Mode Microplate Reader).

Immunoblotting

Proteins in denatured platelet or HDBEC lysates were separated by sodium dodecyl sulfate-polyacrylamide gel electrophoresis (SDS–PAGE) and blotted onto polyvinylidene difluoride membranes. APOLD1 C-term (1 μg mL^{-1}, ab105079, Abcam), GAPDH (1 μg mL^{-1}, #5174 (D16H11), Cell Signaling Technology), VWF (1 μg mL^{-1}, A0082, DAKO), ANGPT2 (1 μg mL^{-1}, AF623, R&D Systems) were probed with the respective antibodies and detected using horseradish peroxidase-conjugated secondary antibodies (0.375 μg mL^{-1}, all from Jackson Immuno-Research) and enhanced chemiluminescence solution (WP20005, Thermo-Fisher Scientific). Membranes were visualized using a ChemiDoc MP imaging system (Biorad).

VWF, ANGPT1 and ANGPT2 ELISA

VWF and ANGPT2 secretion into the supernatant of control and APOLD1-silenced HDBECs was assessed by ELISA according to the manufacturer's protocol. Briefly, 48 h after the first round of transfection media was replaced by fresh complete ECGMV2. After another 48 h supernatants were collected, centrifuged for 20 min at 4°C and 1000 g and the cleared supernatants processed for Angiopoietin 2 Human ELISA (KHC1641, Thermo-Fisher Scientific) and VWF Human ELISA (EHVWF, Thermo-Fisher Scientifc). For determination of plasma ANGPT1 and ANGPT2 levels, plasma was cleared by centrifugation for 30 min at 4°C and 5000 g and subsequently processed for Angiopoietin 1 Human ELISA (EHANGPT1, Thermo-Fisher Scientific) and Angiopoietin 2 Human ELISA (KHC1641, Thermo-Fisher Scientific) according to the manufacturer's protocol. Absorbance at 450 nm was detected using a microplate reader (Synergy™ HTX Multi-Mode Microplate Reader) and concentrations were calculated based on the provided protein standards; curve fitting was done with GraphPad Prism 7.

Whole exome and Sanger sequencing

Whole exome sequencing was performed in 2016 on an Illumina HiSeq2000 instrument using the Agilent SureSelect Human All Exon V5 kit and outsourced at Eurofins Genomics (https://www.eurofinsgenomics.eu/).

Sequenced reads were mapped to the human genome hg19 reference sequence using the BWA software[1] (version 0.7.12). Duplicates were removed using Picard (version 1.104; http://bio-bwa.sourceforge.net/) while sequenced data with read depth lower than 20 were excluded. Variant calling and recalibration were performed using the GATK suite[2] (Version 2.3) following the recommended guidelines (https://www.broadinstitute.org/gatk/guide/best-practices). Identified variants were then annotated with ANNOVAR.

To comply with the anticipated autosomal dominant mode of inheritance of the observed IBD, we selected as candidate causal variation any rare variation that had never been reported in any public database (ExAC, 1000G, etc) or at very low allele frequency (<1%) at the time of analysis and that were present at the heterozygous state in the three whole exome sequenced affected individuals but not present in the two healthy relatives. We further focused on variants located in exonic regions that were likely functional (nonsense, missense, splice, frameshift), leading to 19 rare candidate variants. The predicted deleteriousness of selected candidates was then assessed using the online DNA variant interpretation "Mobidetails" platform (https://mobidetails.iurc.montp.inserm.fr/).[3] Two candidates were predicted to have probable deleteriousness (APOLD1:NM_001130415:exon2:c.C145T:p.R49W; and HS3ST4:NM_006040:exon2:c.G1336T:p.D446Y). *HS3ST4,* encoding the enzyme heparan sulfate D-glucosaminyl 3-O-sulfotransferase 4, was not considered as candidate on the basis of its function. Visual inspection of these candidates using IGV[4] revealed the presence of a common SNP c.146G>A; p.R49Q adjacent to the *APOLD1* rare variant, the combination of which leading to a premature stop codon.

Segregation analysis of both the common c.146G>A variant and the rare c.145C>T substitution in *APOLD1* was performed on DNA from family members of three generations by direct sequencing using the Sanger technique. Variants were named in accordance with the international nomenclature guidelines of the human Genome Variation Society (http://varnomen.hgvs.org/).

Image acquisition

All presented confocal images were acquired using a Leica SP8 inverted microscope equipped with a white light laser and represent maximum intensity projections of z-stacks. The following objectives were used: HC FLUOTAR L 25× /0.95 W VISIR and HC PL APO CS2 63× /1.30 GLYC objectives and LAS-X software version 3.5.5.19976 (Leica Microsystems).

Image analysis

APOLD1 immunolabeling (Figure 1A) was subjected to post-processing with the super-resolution radial fluctuations (SRRF) algorithm[5]. Cell size and shape descriptors (Aspect ratio = major axis : minor axis) of control and *APOLD1*-silenced HDBECs (Figure 2C-D) were quantified by thresholding junctional VE-Cad staining, with subsequent analysis of the binary single channel image using the "analyze particles" plugin of Fiji ImageJ. Each result output was manually controlled. Corrected total cell fluorescence (CTCF) in Figure 2E Supplemental Figure 3C-E was determined using Fiji ImageJ by subtracting the averaged area background from the integrated density (area multiplied by the mean gray value). Densitometric analyses of immunoblots (Figure 3B, 5B-D, 6C, Supplemental Figure 2C, 5E-F, 7) were performed with the help of Fiji ImageJ (version 2.0.0-rc-68/1.52e, http://imagej.nih.gov/ij/, NIH) and represent mean ± standard deviation of at least three immunoblots. SQSTM1, LC3B, VWF, and ANGPT2 positive areas in Figure 4C-D and Supplemental Figure 3F-G, 5B-C were quantified as pixels per area with fluorescence intensity above a threshold value using a single threshold value for all samples within an experiment. Co-localization of proteins (Pearson coefficient displayed in Figure 4E-F, Supplemental Figure 4C-D) was assessed using the indicated immunolabeling as mask with the help of the Coloc-2 plugin in Fiji ImageJ.

SUPPLEMENTAL TABLES

Supplemental Table 1: Clinical and basic hematological characteristics of affected family members. F, female; M, male; n/a, not applicable; TIA, transient ischemic attack; MI, myocardial infarction; YO, years old

Patients	PM4	PM6	PM9	PM11
Gender	F	F	F	M
Year of birth in 3-year bins	1947/ 1950	1943/ 1946	1972/ 1975	1979/ 1982
Platelet count [x10^9 L^{-1}]	208	232	191	189
Mean platelet volume [fL]	8.7	8	8.8	8.8
Leukocyte count [x10^9 L^{-1}]	5.21	6.41	3.80	5.82
Blood group/Rhesus factor	A-	A+	A-	A+
Hemoglobin [g dL^{-1}]	15.8	14.6	13.7	16.2
Ivy Bleeding time [min] Reference range <10 min	3.35	7	6.30 - 10	9.30
Bleeding score ISTH-bat	15	7	12	6
Spontaneous bleeding	Cutaneous, oral cavity, menorrhagia	Cutaneous, menorrhagia, gastro-intestinal, hemoptysis	Cutaneous, menorrhagia, gastro-intestinal	Cutaneous, severe epistaxis, bleeding upon minor injury
Bleeding during surgery	Not constant; bleeding during cholecystectomy surgical curettage	Not constant; bleeding during tooth extraction	Moderate bleeding during tonsillectomy	Bleeding during tooth extraction
Bleeding during delivery	Severe bleeding	Not significant	Severe bleeding (caesarean section)	n/a
Bleeding induced by medication	Progesterone, vasodilator (piribedil)	Aspirin, vasodilator (piribedil)	Vasodilator (dihydroergo cristine)	Aspirin
Ischemic syndromes	Raynaud syndrome	Unexplained transient aphasia without MRI abnormalities TIA: 64 YO MI: 69 YO	Desmopressin has triggered livedo reticularis of legs, Raynaud syndrome	n/a

Supplemental Table 2: Platelet function and VWF characterization.[6] The presented results are representative of repetitive investigations performed in several expert centers using a large range of agonists and various concentrations. On each instance the results showed normal values and variation. LTA: light transmission aggregometry; ADP: adenosine diphosphate; AA: arachidonic acid; TRAP: thrombin receptor activating peptide; A23187: calcium ionophore; plts: platelets; PFA100: platelet function analyzer; Col I: collagen I; Epi: Epinephrin; VWF: von Willebrand factor; RCo: ristocetin cofactor; Ag: related antigen; N, normal; n/a, not applicable.

Analysis	Agonists	PM4	PM6	PM9	PM11	Controls
LTA [%]	ADP 10 µM	80	85	75		77 ± 7
	AA 500 µg mL^{-1}	78	78	75		78 ± 8
	Collagen I [µg mL^{-1}]	82 (2 µg)	85 (2 µg)	67 (2.5 µg) 75 (10 µg)		77 ± 8 (2 µg)
	TRAP 50 µM	85	88	75		78 ± 7
	Convulxin 200 pM	85	88			78 ± 5
	A23187 5 µM	82	85			
	Epinephrine 4 µM	85				
	Ristocetin 1.5 mg mL^{-1}	85	88	75		76 ± 8
	Ristocetin 0.5 mg mL^{-1}	3	3	2		2 ± 2
ATP secretion [nM per 10^{10} plts]	ADP 10 µM	174	213			265 ± 69
	Collagen I 2 µg mL^{-1}	124	66			152 ± 40
	TRAP 50 µM	186	246			226 ± 43
PFA100 [s]	Col I/Epi	144	128	106		<145
	Col I/ADP	80	88	N		<80
VWF	VWF:RCo [%]	>200	198	138	>200	50 - 150
	VWF:Ag [%]	186	127	157	186	50 - 150
	Multimer pattern	N	N	n/a	N	
ANGPT1	Plasma levels [pg mL^{-1}]	1194	1463	n/a	1135	2893 ± 457
ANGPT2		2231	2490	n/a	1935	1189 ± 77
ADAMTS 13	Plasma FRETS-VWF73 activity [%]	109	96	n/a	73	50-150
t-PA	Plasma levels [ng mL^{-1}]	7	4	n/a	5	2-8

Supplemental Table 3: Platelet receptor surface prevalence.[6] Results are expressed as mean fluorescence intensities; n/d, not determined

Receptor (MoAb used)	PM4	PM6	PM9	Controls
	Unstimulated platelets			
αIIbβ3 (AP-2)	58	52	52	47
GPIb (BX-1)	72	78	80	61
P-Selectin (5H10)	3	3	3	2
Activated αIIbβ3 (PAC-1)	3	3	n/d	2
GPVI (3.J/24.J)	9	11	n/d	7
	Activated platelets (TRAP 50 µM)			
αIIbβ3 (AP-2)	86	97	81	77
GPIb (BX-1)	55	42	53	51
P-Selectin (5H10)	13	10	12	14
Activated αIIbβ3 (PAC-1)	17	9	n/d	12

Supplemental Table 4: List of additional variants detected by whole exome sequencing in three affected family members (PM4, PM6 and PM9) but absent in DNA samples from unaffected family members (PM12 and PM13). HGVS, Human Genome Variant Society; Polyphen 2, Polymorphism Phenotyping v2 prediction. NA, not annotated with Mobidetails.

Gene	HGVS DNA on transcript	HGVS protein	HGVS genomic (Hg38)	EXAC_ALL	rsID	SIFT	Polyphen 2	ClinPhred
HS3ST4	NM_006040.2:c.1336G>T	NP_006031.2:p.(Asp446Tyr)	chr16:g.26136213G>T	5.11E-05	rs775777458	**Damaging**	**Probably damaging**	**Damaging**
ADGRF3	NM_001321971.1:c.2351A>G	NP_001308900.1:p. (Tyr784Cys)	chr2:g.26534041T>C	0.0148	rs115282281	**Damaging**	**Probably damaging**	Tolerated
BAZ2A	NM_001300905.1:c.2207G>A	NP_001287834.1:p. (Arg736Gln)	chr12:g.56606299C>T	0.0012	rs139817454	Tolerated	**Probably damaging**	Tolerated
NFATC4	NM_004554.4:c.1934C>T	NP_004545.2:p.(Thr645Met)	chr14:g.24375979C>T	0.0104	rs45570732	Tolerated	**Probably damaging**	Tolerated
RNF180	NM_001113561.2:c.1168C>T	NP_001107033.1:p.(Arg390Cys)	chr5:g.64214494C>T	0.0005	rs568069088	**Damaging**	**Probably damaging**	Benign
PRSS36	NM_173502.4:c.1873G>A	NP_775773.2:p.(Val625Ile)	chr16:g.31141497C>T	0.0083	rs117442264	**Damaging**	Benign	Tolerated
XPO6	NM_015171.3:c.1625C>T	NP_055986.1:p.(Thr542Met)	chr16:g.28125830G>A	0.0005	rs201657764	**Damaging**	**Probably damaging**	Tolerated
GLG1	NM_001145667.1:c.3338A>T	NP_001139139.1:p. (Asn1113Ile)	chr16:g.74456683T>A	0.0005	rs144493700	Tolerated	**Possibly damaging**	Tolerated
AARS1	NM_001605.2:c.1685C>T	NP_001596.2:p.(Thr562Ile)	chr16:g.70261144G>A	0.0049	rs148355156	Tolerated	Benign	Tolerated
MYT1	NM_004535.2:c.2345C>G	NP_004526.1:p.(Thr782Ser)	chr20:g.64221996C>G	0.0165	rs78568430	Tolerated	Benign	Tolerated
FST	NM_013409.2:c.454G>C	NP_037541.1:p.(Glu152Gln)	chr5:g.53483680G>C	0.0043	rs11745088	Tolerated	Benign	Tolerated
MLKL	NM_152649.3:c.394T>C	NP_689862.1:p.(Ser132Pro) H	chr16:g.74695364A>G	0.0139	rs35589326	Tolerated	**Probably damaging**	Tolerated
TAS2R43	NM_176884.2:c.460C>T	NP_795365.2:p.(Arg154Trp)	chr12:g.11091770G>A	0.0088	rs200586631	Tolerated	Benign	Tolerated
HELZ2	NM_001037335.2:c.5311G>A	NP_001032412.2:p.(Val1771Ile)	chr20:g.63563511C>T	0.0006	rs369651267	Tolerated	Benign	Tolerated
OR8U1	NM_001005204.1:c.799G>T	NP_001005204.1:p. (Ala267Ser)	chr11:g.56376422G>T	0.0027	rs373392784	Tolerated	Benign	Tolerated
PRAMEF4	NM_001009611.4:c.1326C>G	NP_001009611.2:p. (Asn442Lys)	chr1:g.12879655G>C	0.0003	rs149134171	Tolerated	Benign	Tolerated
CTSZ	NM_001336.3:c.707C>T	NP_001327.2:p.(Thr236Ile)	chr20:g.58996733G>A	0.00004708	rs201551005	Tolerated	Benign	Tolerated
SSPO	NM_198455:c.G4475A	NP_940857.2:p.Cys1492Tyr	chr7:149789613G>A	0.0006	rs202159011	NA	NA	NA

Supplemental result: Procoagulant activity and microvesiculation of platelets.[7] Procoagulant activity and microparticle formation of platelets from PM4 and PM9 was assessed by flow cytometry after activation of platelets.

The tests included measurement of prothrombinase activity using the chromogenic substrate S2238, and formation of microparticles using annexin V-FITC by flow cytometry

a) Without stimulation: results for the ionophore A23187 (1 µM and 3 µM) and Ca^{2+}-ATPases inhibitors (Thapsigargin: 0.3 µM and 3 µM; cyclopiazonic acid 100 µM) were normal.
b) Upon stimulation with 0.1 U mL^{-1} and 0.5 U mL^{-1} thrombin, 10 µg mL^{-1} collagen or a mixture of both results were also normal.

In addition, the kinetics of aminophospholipid exposition measured by the binding of annexin V-FITC in response to stimulation with the A23187 ionophore were also unaltered.

SUPPLEMENTAL FIGURES

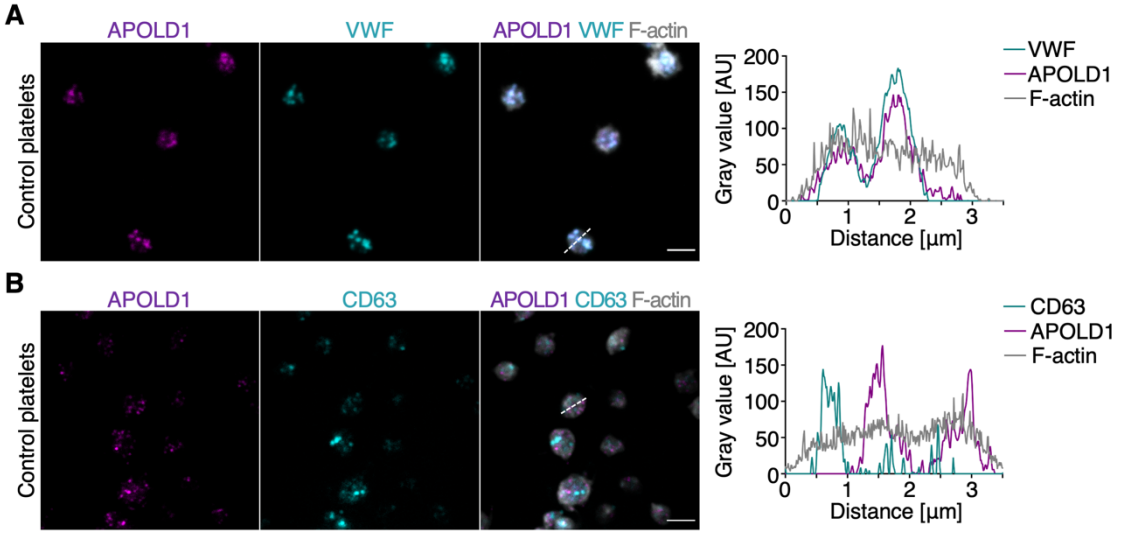

Supplemental Figure 1: APOLD1 localizes to platelet α-granules. A-B) Resting platelets of healthy controls were allowed to adhere to a poly-L-lysine-coated surface and processed for immunolabeling for the indicated proteins. Subsequently, samples were analyzed by confocal microscopy. Histograms represent fluorescence intensity along the dashed lines. Scale bars, 3 µm.

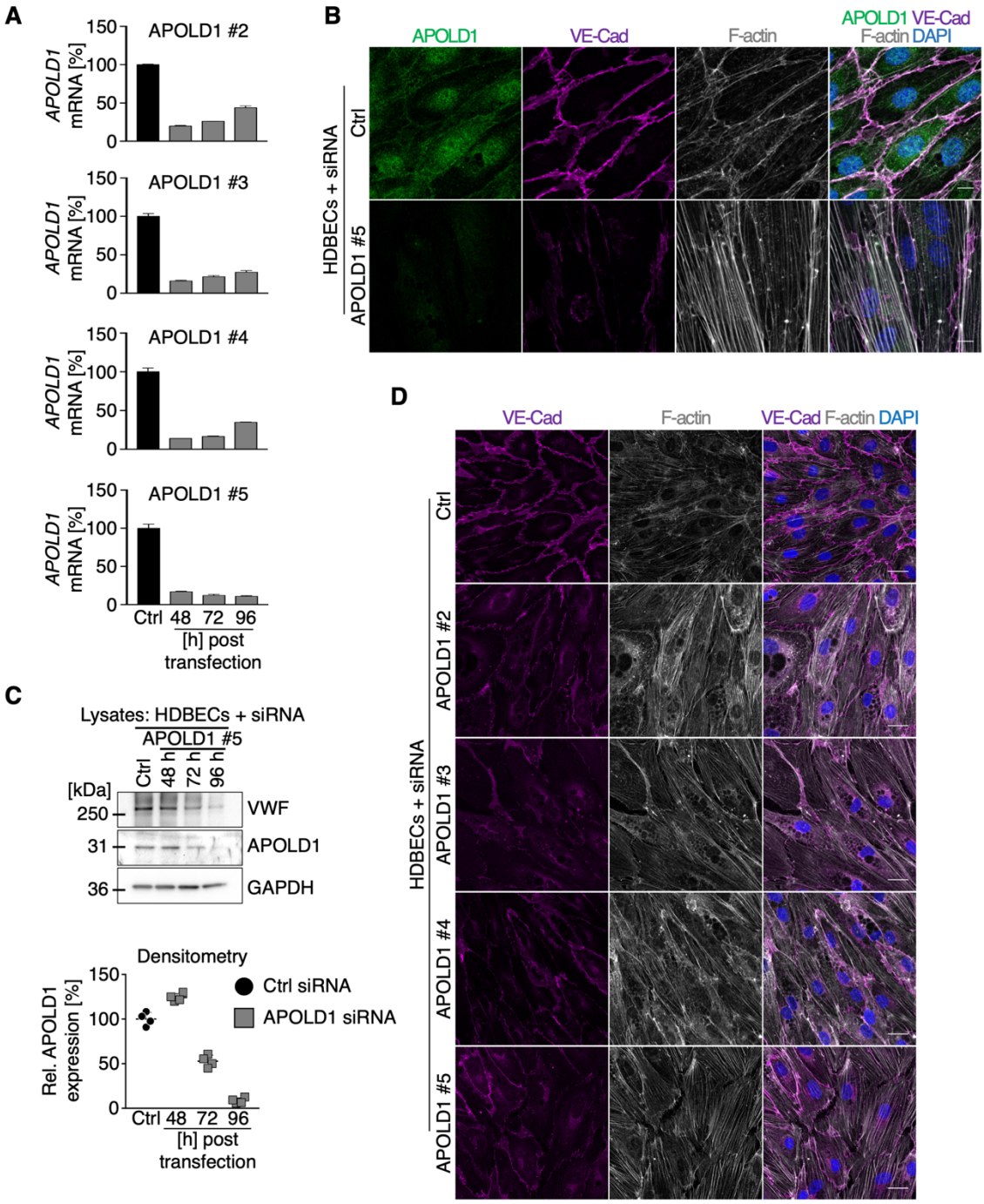

Supplemental Figure 2: Efficient silencing of *APOLD1* in HDBECs. A) *APOLD1* expression of control and *APOLD1* siRNA-treated human dermal blood endothelial cells (HDBECs) was analyzed by reverse transcription real time PCR (qPCR). Results represent mean ± s.d. of at least four independent experiments. **B)** Control or *APOLD1* siRNA-treated HDBECs were immunolabeled for APOLD1 (green), VE-Cad (magenta), and F-actin (gray). Nuclei were highlighted with DAPI (blue). Scale bars, 10 µm. **C)** Proteins from control and *APOLD1* siRNA #5-treated HDBECs were extracted at different time points after siRNA transfection and processed for immunoblotting and densitometric analysis. **D)** All four tested siRNAs (#2 - #5) directed against the *APOLD1* transcript result in similar morphological changes such as junctional (VE-Cad) and cytoskeletal (F-actin) alterations that ultimately translated into an altered cell shape and size. Nuclei were labeled with DAPI. Scale bars, 25 µm. Immunoblots and confocal microscopic images are representative of at least three independent experiments.

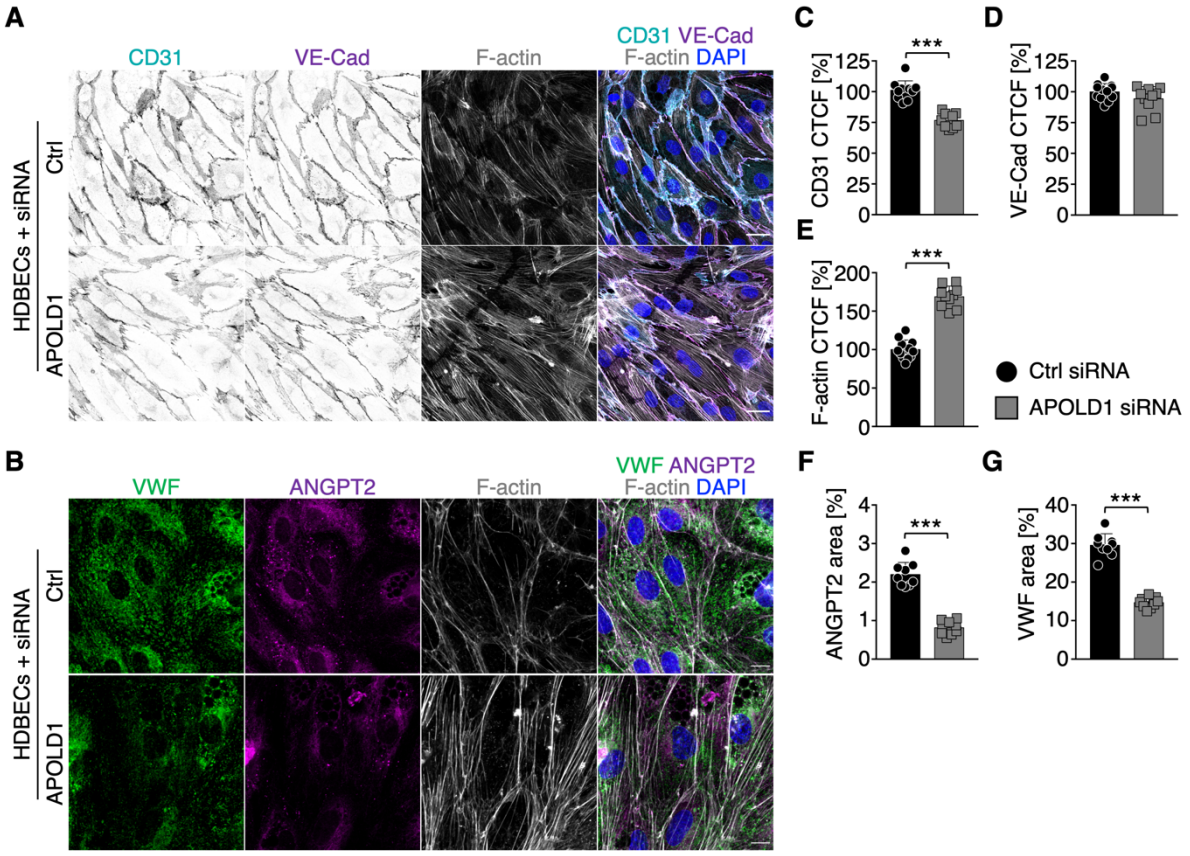

Supplemental Figure 3: 50% loss of APOLD1 alters endothelial cytoskeletal as well as junctional organization and WPB biology. A-B) *APOLD1* silencing in HDBECs alters the organization of cell-cell junctions (platelet-endothelial cell adhesion molecule 1, PECAM1/CD31; vascular endothelial cadherin, VE-Cad;) as well as cytoskeletal architecture and WPB cargo content (angiopoietin-2, ANGPT2; von Willebrand factor, VWF). **C-E)** Image analysis revealed reduced immunolabeling intensities (corrected total cell fluorescence, CTCF) of the junctional proteins (**C**) PECAM1/CD31, (**D**) alterations of VE-Cad distribution as well as enhanced (**E**) actin stress fiber formation. Each symbol represents the average of at least 100 cells. Pooled data from three independent experiments is displayed **F-G)** Decreased content of WPB cargoes VWF and ANGPT2 upon 50% loss of APOLD1. Each symbol represents one analyzed (n = 9) image from three independent experiments. Data represent mean ± s.d.

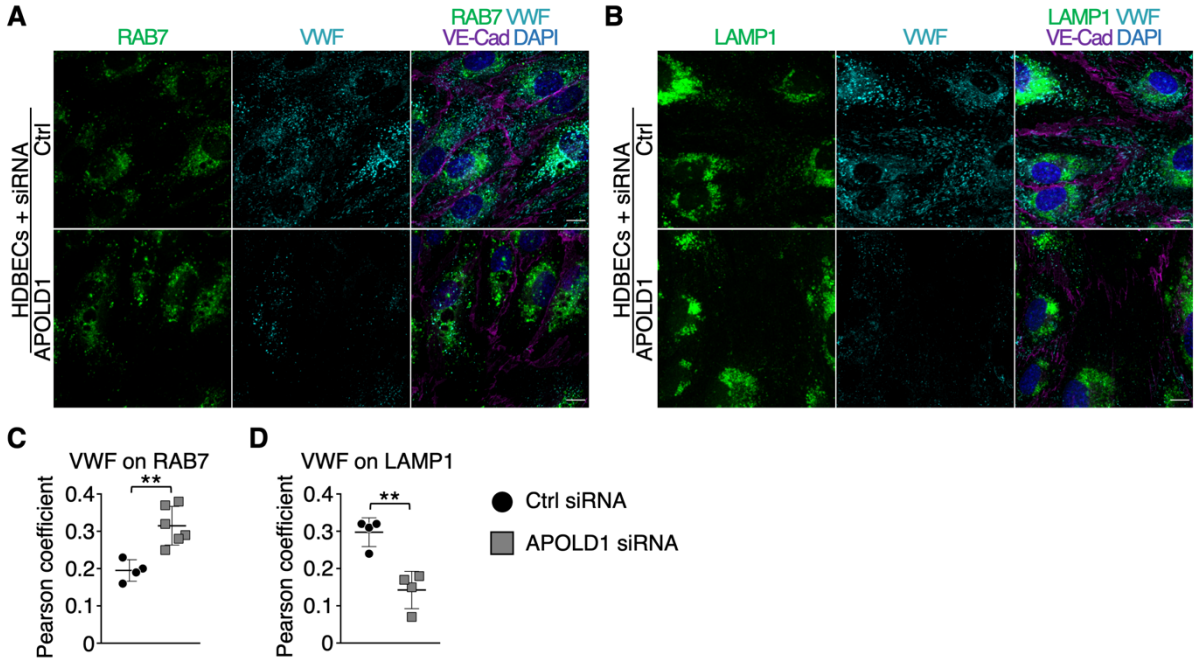

Supplemental Figure 4: Loss of APOLD1 perturbs endo-lysosomal processing of VWF. A-B) Immunolabeling and subsequent image analysis of control or *APOLD1* siRNA-treated HDBEC monolayers reveals an increased localization of VWF to (**A, C**) RAB7-positive secretory granules, but a decreased co-localization to (**B, D**) degradative LAMP1-positive vesicles upon *APOLD1* silencing. Each symbol in **C-D** represents one analyzed ($n \geq 4$) image. Horizontal lines indicate mean ± s.d. Images are representative of at least three independent experiments. Scale bars, 10 µm. Wilcoxon-Mann-Whitney test, $^{**}P < .01$.

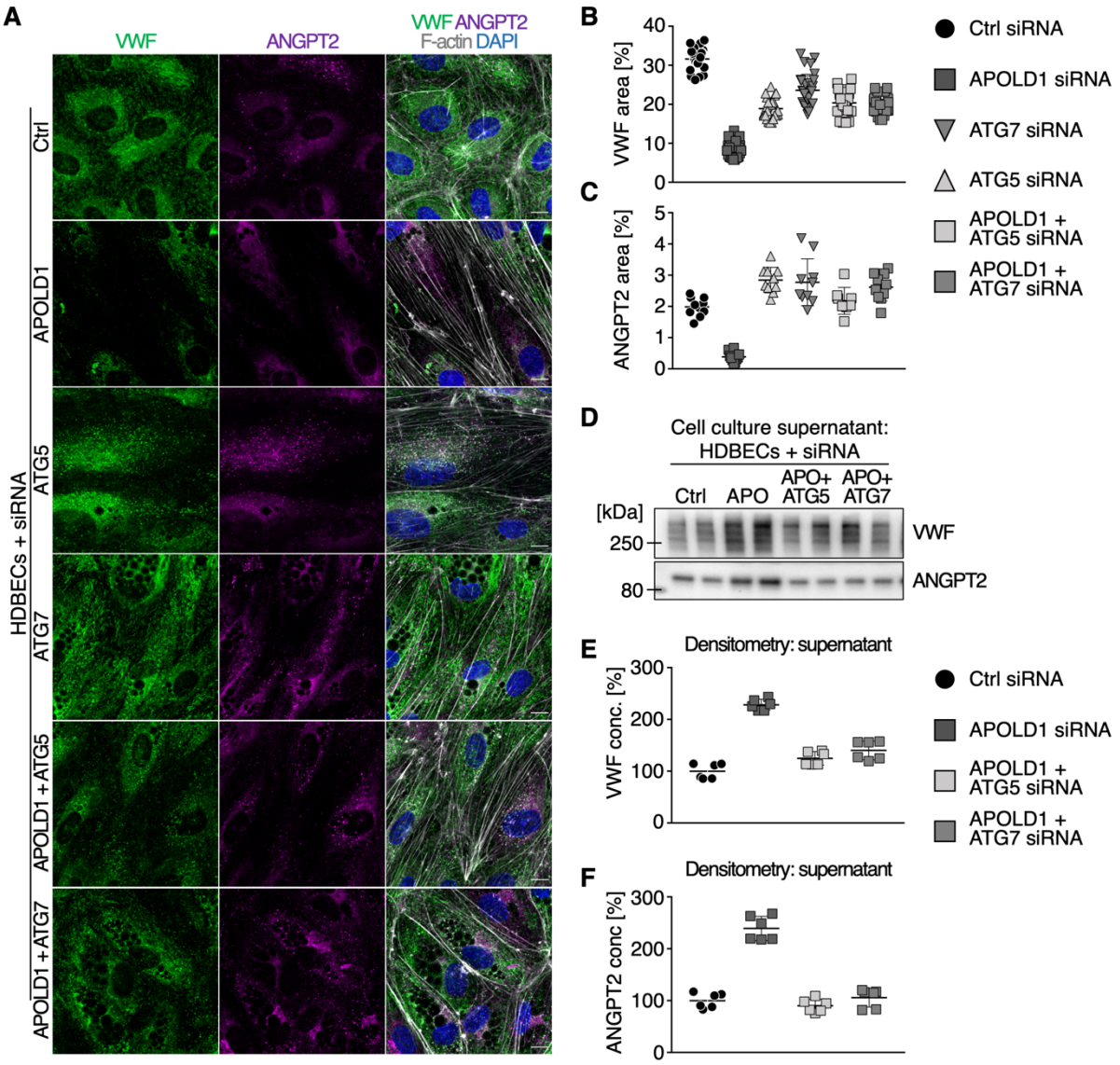

Supplemental Figure 5: Secretory autophagy is the major route for WPB release in the absence of APOLD1. A-C) Immunolabeling and subsequent image analysis of control, *APOLD1*, *autophagy related 5* (*ATG5*), *ATG7*, *APOLD1+ATG5*, or *APOLD1+ATG7* siRNA-treated HDBEC monolayers reveals that co-simultaneous silencing of *ATG5* or *ATG7* ameliorates loss of the WPB cargoes von Willebrand factor (VWF) and angiopoietin 2 (ANGPT2) in *APOLD1*-silenced HDBECs. Scale bars, 10 µm. Each symbol represents one analyzed (n ≥ 8) image. Pooled data from three independent experiments is presented. **D-F)** Immunoblotting and subsequent densitometric analysis confirms reduced secretion of VWF and ANGPT2 upon co-simultaneous silencing of *ATG5/ATG7* and *APOLD1*. Images are representative of three independent experiments. Each symbol represents averaged results from one sample (n = 6). Pooled data from three independent experiments is presented. Horizontal lines denote mean ± s.d. Results were analyzed by one-way ANOVA followed by Dunnett's multiple comparisons test, ***$P < .001$.

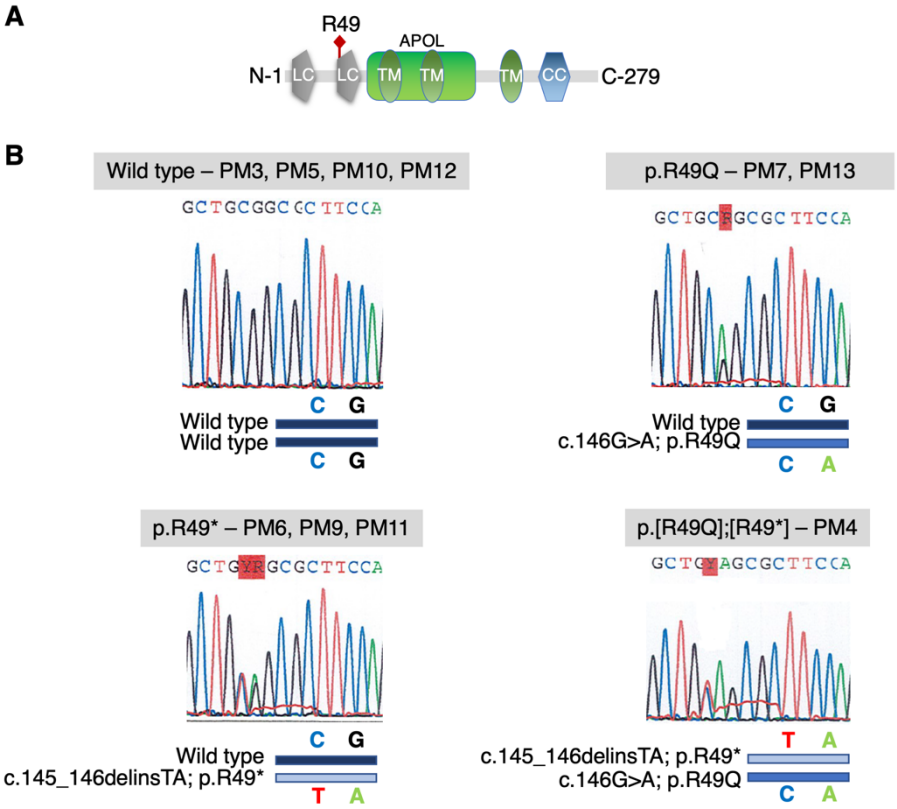

Supplemental Figure 6: Sanger sequencing electropherograms for different pedigree members. **A)** Schematic representation of APOLD1 protein and localization of the premature stop codon at R49*. LC: low complexity region; APOL: Apolipoprotein-like domain; TM: transmembrane domain; CC: coiled-coil domain. **B)** Exemplary Sanger sequencing electropherograms of unaffected (wild type alleles: PM3, PM5, PM10, and PM12; common heterozygous p.R49Q variant: PM7 and PM13), as well as pedigree members suffering from the IBD (p.R49* variant: PM6, PM9, and PM11; p.[R49Q];[R49*] variant: PM4).

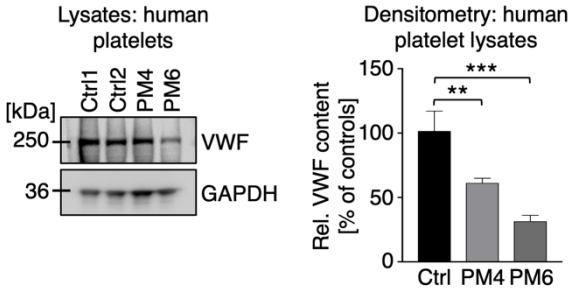

Supplemental Figure 7: *APOLD1*^{R49*} is associated with decreased platelet VWF levels. Reduced VWF content in platelet lysates from pedigree member (PM) 4 and PM6 with an *APOLD1*^{R49*} variant revealed by immunoblotting with subsequent densitometric quantification of VWF expression relative to GAPDH. Immunoblots are representative of three experiments and bars represent mean ± s.d.

SUPPLEMENTAL REFERENCES

1. Li H, Durbin R. Fast and accurate short read alignment with Burrows-Wheeler transform. *Bioinformatics*. 2009;25(14):1754–1760.
2. McKenna A, Hanna M, Banks E, et al. The Genome Analysis Toolkit: a MapReduce framework for analyzing next-generation DNA sequencing data. *Genome Res.* 2010;20(9):1297–1303.
3. Baux D, Van Goethem C, Ardouin O, et al. Correction: MobiDetails: online DNA variants interpretation. *Eur J Hum Genet*. 2021;29(2):361.
4. Robinson JT, Thorvaldsdóttir H, Winckler W, et al. Integrative genomics viewer. *Nat. Biotechnol.* 2011;29(1):24–26.
5. Gustafsson N, Culley S, Ashdown G, et al. Fast live-cell conventional fluorophore nanoscopy with ImageJ through super-resolution radial fluctuations. *Nat Commun*. 2016;7:12471.
6. Nurden P, Bordet J-C, Pillois X, Nurden AT. An intracytoplasmic β3 Leu718 deletion in a patient with a novel platelet phenotype. *Blood Adv*. 2017;1(8):494–499.
7. Dachary-Prigent J, Freyssinet JM, Pasquet JM, Carron JC, Nurden AT. Annexin V as a probe of aminophospholipid exposure and platelet membrane vesiculation: a flow cytometry study showing a role for free sulfhydryl groups. *Blood*. 1993;81(10):2554–2565.